Hand Rehabilitation Dynamic Splint with Variable Force via Pneumatic Artificial Muscle Actuators

Annals of Biomedical Engineering
https://doi.org/10.1007/s10439-026-04233-3

ORIGINAL ARTICLE

Hand Rehabilitation Dynamic Splint with Variable Force via Pneumatic Artificial Muscle Actuators

V. Potnik[1] · G. Frediani[1] · M. Dimitri[1] · F. Carpi[1,2]

Received: 3 October 2025 / Accepted: 1 June 2026

Abstract

Purpose Dynamic hand splints are rehabilitation orthoses equipped with elastic bands/springs that provide passive resistance to finger movements. To enable real-time controllability of rehabilitative exercises and potentially improve therapeutic outcomes, it would be advantageous to replace the elastic components with soft actuators, enabling finger movements to be exercised against controllable loads. The ideal soft actuators for dynamic hand splints should generate large displacements at moderate forces, have a compact size and low specific weight, and be electrically safe.

Methods Here, we describe a dynamic splint embedded with soft pneumatic actuators functioning as "inverse artificial muscles", which elongate when pressurised, reducing the force that resists finger flexions. A prototype system was assembled using off-the-shelf materials. An actuator was fabricated and mounted on a forearm brace, connecting one extremity to a finger via a tendon and the other one to an onboard load cell, to monitor the force exerted during finger motions. The system was tested via two psychophysical tests.

Results A dynamic psychophysical test on perceptual differences in force demonstrated that subjects were able to reliably perceive force variations, with a sensitivity (slope of the psychometric curve) of ~ 110%/bar at 50% probability. In a static psychophysical test with a fully flexed finger, the maximum average force was ~ 5.2 N at 0 bar, whilst the minimum average force when subjects reported no perception of force, by progressively increasing the pressure, was as low as ~ 0.7 N at 3 bar, indicating good accuracy of the system.

Conclusion The developed active splint has the potential to enable dynamically controllable hand rehabilitation tasks.

Keywords Actuator · Rehabilitation · Pneumatic · Orthosis · Hand · Splint

Introduction

To mitigate motor impairments in patients who retain residual ability of finger movement, dynamic hand splints are frequently used as rehabilitation orthoses [1]. They help to increase range of motion [1], reduce joint pain [1], spasticity [2, 3], and soft tissue adhesions [3], prevent muscle atrophy [3], and enhance muscle balance, brain plasticity, and blood circulation [3]. As such, they are considered useful for restoring functional hand movements and supporting effective rehabilitation outcomes in subjects affected by post-stroke impairment, traumatic brain injury, and post-surgical or post-burn tissue stiffening [1–6].

The key components of dynamic hand splints used in clinical practice are elastic bands/springs, which exert passive resistive forces that counteract voluntary finger movements [1–7]. Often, the elastic components run along the dorsal side of the forearm and hand, attaching to the dorsal surfaces of the thumb and fingers, just before the proximal interphalangeal (PIP) joints. The fingers are guided using slings that apply pressure to the palmar side, proximal to the PIP joints, allowing for controlled finger movements [1–5, 7]. Different implementations use elastic bands arranged on the palmar side of the hand to assist finger extensions [6].

Dynamic hand splints share a common limitation: the inability to vary the resistive load in real time, i.e. dynamically,

Associate Editor Jennifer Nichols oversaw the review of this article.

✉ F. Carpi
federico.carpi@unifi.it

[1] Department of Industrial Engineering, University of Florence, Florence, Italy

[2] IRCCS Fondazione Don Carlo Gnocchi ONLUS, Florence, Italy

during the exercise. Whilst variable elastic bands or adjustable torsion springs can be used to change the counteracting force, they lead to intermittent rehabilitation exercises, as adjustments require pausing to modify settings. Conversely, the possibility of transforming the passive structure of a splint into a device that can monitor the task and automatically control the counteracting force, in real time, could significantly extend the functionality and potentially also the rehabilitation outcomes. This would require 'active' splints, where the elastic bands/springs are replaced with wearable actuators. They would allow for tailoring the rehabilitation task, not only before but also during the treatment, according to dynamic rehabilitation strategies, as well as the patient's actual performance.

To implement such active dynamic hand splints, ideal actuators should have suitable properties, including stretchability (softness), ability to combine large displacements with moderate forces, a lightweight and compact structure, a low specific weight, as well as possibly a low cost. This study aims to describe a new technology that combines such requirements, to enable effective active splints.

The state-of-the-art does not offer straightforward solutions to implement them. Indeed, most of the systems described in the literature dealing with actuations of the hand are designed mostly for grasping assistance. Amongst the various actuation technologies used for that purpose [8–12], one of the most typical consists of electromagnetic motors connected to fingers via tendons [13–18]. Some such systems are commercially available, such as the Gloreha Hand Rehabilitation Glove (Idrogenet Srl, Brescia, Italy) [19, 20]. Whilst such motor-based systems are capable of high actuation performance, they have noticeable limitations in terms of wearability and portability, as they typically require bulky and heavy mechanical driving units, grounded next to the patient. Other actuation technologies used for hand orthoses include shape memory alloy actuators [21–24], and twisted-and-coiled polymer actuators [25]; both of them, however, have electrothermal activation, which limits the energy efficiency and actuation speed.

A large number of exoskeletons for the hand employ soft pneumatic or fluidic devices [8, 26–30]. In particular, to implement gloves capable of grasping assistance, various kinds of pneumatic actuation systems are under investigation, covering a diversity of actuator configurations, including fishbone-inspired structures [31], bending types [32–34], origami shapes [35], fabric-based architectures [36, 37], fibre-reinforced chambers [38], and bellows [39–41]. Some of these exoskeletons have also been developed with motion sensors incorporated in the structure of a glove [42–44]. When actuation is needed along a line, the traditional McKibben configuration is usually the first choice, as it enables linear contractions and radial expansions; accordingly, such devices are typically referred to as pneumatic artificial muscle actuators [45–48]. McKibben actuators have been applied, for instance, to suppress the effects of hand tremors and for grasping assistance [49–51]. Linear pneumatic actuators can also be implemented with 'inverse' operation, i.e. by making them elongate, rather than contract, upon pressurisation; to that end, an elastomeric inflatable tube surrounded by a coil, which restricts radial expansions upon inflation, enabling only linear elongations; as a result, such devices are often referred to as pneumatic inverse artificial muscle actuators [52–54]. Fluidic versions of such actuators have been used in gloves for grasping assistance [55]. Alongside McKibben actuators, bending-type soft pneumatic actuators have recently become increasingly common in hand rehabilitation applications. One example is a segmented-chamber design, in which the chambers are arranged to follow the natural trajectory of a human index finger. This bending motion, enabling both flexion and extension assistance, is achieved through a honeycomb-like structure of the chambers [56].

The wide variety of actuation technologies (either rigid or soft) described above is typically used for hand grasping rehabilitation. In contrast, this study was motivated by the need for technologies that can fulfil a different rehabilitation task: resisting voluntary flexions of the fingers, with loads that can be controlled dynamically. This is aimed at enabling active versions of conventional passive hand splints [57]. Such envisaged active splints aim to achieve enhanced therapeutic outcomes, owing to the possibility of adapting (personalising) the counteractive load, both before and during the rehabilitative task.

To the best of our knowledge, only a few studies have targeted active dynamic splints to date. Some of them have been conceived to combine a soft, lightweight and compact structure with purely electrical activation, using dielectric elastomer actuation [58–61]; nevertheless, such attempts so far have always been limited by the need for high driving voltages and by the fact that force outputs are usually lower than those achievable with technologies that adopt bulkier actuators, such as electromagnetic motors and pneumatic systems driven by external compressors.

Within such a context, here we present the use of pneumatic inverse artificial muscle actuators to demonstrate an active dynamic hand splint, whose performance was characterised with both mechanical and psychophysical tests. The active dynamic hand splint was conceived as a wearable structure equipped with the soft pneumatic actuators, which could be stretched by a finger upon voluntary changes of position from extension to flexion, as represented in Fig. 1.

During stretching, the actuator exerts a variable hyperelastic resistance, according to a stress–strain characteristic relationship that can be electro-pneumatically controlled, to accommodate different rehabilitation needs. The device is intended for use in clinical settings under the supervision of a therapist. The therapist will be responsible for setting up

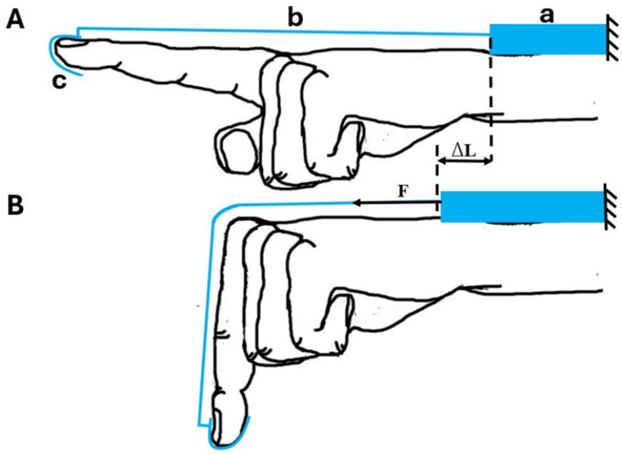

Fig. 1 Conceptual drawings of the use of a soft wearable actuator serving as a variable-load active component for a dynamic hand splint. The actuator **a** was pulled by a finger via a tendon **b**, connected to the finger via a cap **c**. By changing the finger position from extension **A** to flexion **B**, the actuator was elongated (ΔL) by an applied force (F), offering a hyperelastic resistance, which can be controlled electro-pneumatically

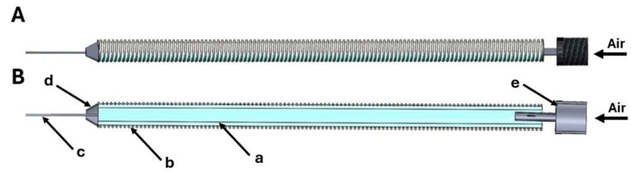

Fig. 2 Lateral-view **A** and cross-sectional-view **B** drawings of the pneumatic inverse artificial muscle actuator used to implement the active dynamic splint, showing the various parts of the device: **a** elastomeric tube, **b** plastic coil, **c** metal tendon, **d** plastic cap, and **e** air needle

the device on the patient and ensuring it is operated safely and correctly during therapy sessions.

The actuator's technical specifications were identified as follows. The maximum elongation ΔL (Fig. 1) was defined by measuring on a group of adult volunteers the displacement of a tendon connected to a finger, when the latter changed position from extension to flexion; displacement values were found to be in the range 20–30 mm, depending on the subject's hand size. Therefore, a maximum elongation of 30 mm was considered as a worst-case specification. The maximum force F (Fig. 1) was defined according to the literature, which showed that passive splints usually apply approximately 3 N per finger [62–64]. Accordingly, a maximum elongation of 30 mm and a maximum force of 3 N were used as reference values to design the actuator and splint, as described in the next section.

Materials and Methods

Pneumatic Actuator Fabrication

Figure 2 presents schematic drawings of the actuator that was used to create the active dynamic hand splint.

The actuator was assembled with materials and processes previously described by us [52]. In particular, the actuator had an active length of 100 mm and was made of an off-the-shelf 40-ShoreA silicone elastomeric tube (LegenDay Technology Co, China), having outer and inner diameters of 5 and 3 mm, respectively. The tube was sealed with a 0.5 mm-thick polypropylene film, bonded with a glue (Loctite 495), and was surrounded by a 0.5-mm-thick Nylon filament coil. The latter prevented the tube from radially expanding upon inflation to maximise the actuator's elongation.

Active Splint Design and Assembly

Figure 3 presents drawings and a collage of photos of the active splint's structure and operation, when the actuator was

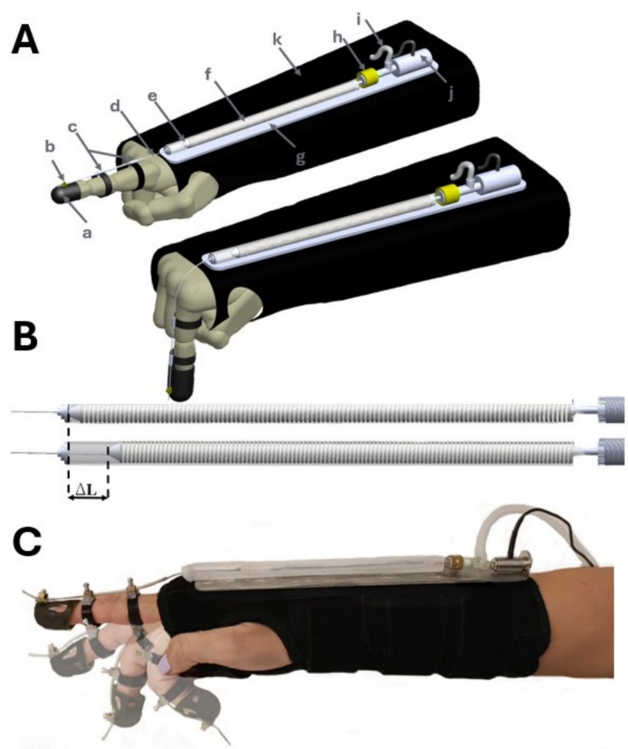

Fig. 3 Drawings **A**, **B** and combined photos **C** of the active dynamic splint in action (see the Supplementary Video S1). A finger was connected to a pneumatic inverse artificial muscle actuator. The latter offered a controllable force when it was elongated **B** by voluntary movements of the finger, from a fully extended state to a flexed state **A**, **C**. The main constitutive parts of the structure were: **a** finger cap; **b** tendon fixing screw; **c** Velcro ring with tendon guide cylinder; **d** tendon; **e** actuator guide tube; **f** actuator; **g** support rigid slab; **h** air needle and connector; **i** air tube; **j** load cell; **k** fabric brace

stretched by finger flexion. A movie of the system in action is provided as Supplementary Video S1.

The actuator was lodged inside a larger silicone elastomeric tube (having an inner diameter of 9 mm and a length of 165 mm), serving both as a protection case and as a guide to maintain an axial direction of deformation for the actuator. The guiding tube was glued to a 220-mm-long, 26-mm-wide, and 2 mm-thick aluminium slab, serving as a rigid substrate to firmly and coaxially stabilise the encased actuator, its pneumatic connector and a load cell (FLAE–10N, Forsentek, China), as shown in Fig. 3. The load cell, which was used to measure the force applied by the finger, was electrically connected to an external amplifier and analogue-to-digital converter (HX711 module, AVIA, China), and a microcontroller (Arduino Uno: ATmega328P, Arduino, Italy), which was interfaced to a personal computer. The load cell was attached to the actuator's rear end, which was also fitted with an air needle and a connector for air inlet, via soft silicone tubing.

The slab was attached to a fabric brace, which immobilised the forearm, wrist and a part of the hand (Fig. 3). The whole brace surface was fitted with Velcro, which not only made the structure easily adaptable via straps to different hand sizes but also allowed the actuator-carrying slab (previously glued to Velcro stripes) to be easily attached and repositioned, according to the finger to be exercised.

The actuator's front end was connected to the finger via a 0.8 mm-thick steel tendon, which was encased in a 2 mm-thick polyurethane tube, to avoid harmful friction between the metal wire and the skin. The tendon was attached to the finger via a plastic cap, which was made adaptable to different finger sizes, by means of a soft rubber insert. The tendon's length was made adjustable to the finger's length, by securing the tendon to the plastic cap via a metal cylinder with a screw. The tendon was maintained aligned along the finger, by routing it through tiny cylinders secured to the finger via Velcro rings.

The actuator was pneumatically activated by a compressor (FD-186 Piston Type 125W Air Compressor, Fengda, Italy).

Pneumatic Actuator Mechanical Characterisation

Bench testing was performed on actuator samples, to obtain a stress-strain characterisation within the elongation range (0–30 mm) that they were expected to experience onboard the splint, at different pressures. By considering that in the splint the finger's transition between full extension and full flexion would typically take at least ~ 1 s (higher speeds are not realistic for patients requiring rehabilitation), the tensile tests were accomplished at a speed of 30 mm/s.

The measurements were performed with a dynamometer (model Z0.5, Zwick/Roell, Switzerland), on three actuator samples, nominally identical. Each actuator was initially pre-strained by 10 mm (with a tensile speed of 10 mm/s), to mimic a typical condition occurring in the splint, where the actuator was pre-tensioned. Then, the actuator was inflated at a given pressure, chosen within a set of values in the range 0–3 bar, with 0.5 bar increments. Afterwards, the pressurised actuator was pulled, to further elongate it by additional 30 mm, and then released back to the initial pre-elongation. To achieve a stabilisation of the elastomer's viscoelastic response (Mullin's effect), five consecutive cycles were accomplished

Pneumatic Actuator Mechanical Modelling

A finite element model of the actuator was developed to perform quasi-static simulations of the force generated in response to imposed displacement and internal pressure. The model was created using commercial software (Simulia, 3D Experience, Dassault Systèmes, France). The simulations were conducted under quasi-static assumptions, neglecting inertial and damping effects, and using the implicit nonlinear solver. Equilibrium equations were incrementally solved using a Newton–Raphson iterative scheme. Loads and boundary conditions were applied progressively through time-controlled steps, allowing the solver to follow the nonlinear response of the system whilst maintaining numerical stability. Automatic time incrementation was enabled, to ensure adaptive adjustments of the increment size based on convergence performance. A near-incompressibility condition was imposed through a penalty-based incompressibility formulation, ensuring numerical stability whilst maintaining realistic deformation patterns.

The finite element geometry was discretised using three-dimensional tetrahedral solid elements, selected for their robustness in handling complex geometries and large deformations. The element formulation was based on a displacement-based approach with numerical integration performed at Gauss points within each element. The mesh density and refinement strategy were selected to ensure accurate representations of deformation gradients, whilst preserving computational efficiency; in particular, the mesh consisted of element sizes ranging from 0.5 to 0.05 mm, with local refinements in high-stress regions to minimise discretisation errors.

Several assumptions were introduced to achieve a trade-off between mechanical accuracy and computational efficiency. The function of the containment coil (radial constraint) was modelled by imposing a sliding constraint on the tube's outer surface. By assuming that in the real actuator the stress exerted by the external containment coil was able to fully counteract the pneumatic pressure along the radial direction, the latter was not simulated. Therefore, the pneumatic pressure was modelled only as an axial force distributed on the cylinder's inner cross-section. Whilst this approach did not capture local pressure distributions, it preserved the pressurisation's mechanical effect along the principal deformation axis, i.e. the direction along which the model was validated using experimental data from bench testing.

The actuator's hyperelastic behaviour was modelled using a fourth-order Ogden strain energy density function W:

$$W = \sum_{i=1}^{N} \frac{\mu_i}{\alpha i}\left(\lambda_1^{\alpha i} + \lambda_2^{\alpha_i} + \lambda_3^{\alpha i} - 3\right), \tag{1}$$

where λ_1, λ_2, and λ_3 are the principal stretch ratios, μ_{i} and α_{i} are material parameters, and $N=4$. The determination of the material parameters would have required fitting the experimental stress–strain curve of the constitutive material. However, as the actuator was assembled starting from a commercial tube, its raw material was not available to create samples suitable for material testing. Therefore, for simplicity, the Ogden model parameters were determined by fitting the experimental stress–strain curve of the whole actuator (in its unpressurised state).

They were as follows: $\mu_1=-1.768\times10^6$ N/m^2, α_1=12.005, μ_2=2.94×10^6 N/m^2, $\alpha_2=-25.376$, μ_3=0.768×10^6 N/m^2, α_3 =6.402, $\mu_4=-0.113\times10^6$ N/m^2, and $\alpha_4=-31.223$. The fitting process was performed using the Material Calibration tool available within the Simulia environment.

The quasi-static simulation was composed of three steps: (i) a pre-extension phase, where an imposed displacement of 10 mm was applied to the actuator's free end; (ii) an equivalent pressurisation phase, where an axial force was distributed on the cylinder's inner cross-section; (iii) a final extension phase, where an additional imposed displacement of 30 mm was applied, resulting in a total elongation of 40 mm, to simulate the maximum extension reached experimentally.

Psychophysical Tests

To complement the mechanical characterisation of the actuator, psychophysical investigations were also conducted to assess how the mechanically generated forces were perceived by users. Whilst the mechanical tests provided objective measurements of the actuator's force generation and modulation capabilities, the psychophysical tests provided subjective evidence, as they evaluated the perceptual relevance of these forces. In particular, the investigations assessed the sensitivity to variations in force magnitude and to low-force stimuli close to perceptual thresholds. This complementary approach aimed to verify that the actuator was not only able to produce controllable and predictable resistive forces within the range relevant for dynamic hand splinting but also capable of generating stimuli that can effectively be perceived by users.

Psychophysical Test on Perceptual Differences in Force

To complement the mechanical characterisation, the splint was also studied with psychophysical tests, aimed at investigating how users perceived the reaction forces generated by the device. Specifically, a first type of psychophysical test was conducted to assess the perceptual sensitivity to changes in force as follows. The subject was asked to vary the finger position from full extension to full flexion, when the actuator was driven at a given pressure.

To perform the tests, the splint was connected to the index finger of the dominant hand (the right one for all subjects), paying special attention to ensure proper alignment of the actuator, tendon and finger, by carefully routing the tendon over the knuckles, passing it through the tiny cylinders on the Velcro rings and securing it to the finger cap. The actuator was pre-strained by 10 mm, to keep it straight, avoiding bending.

Amongst the various psychophysical methods typically used to determine a perceptual sensitivity, we chose the classical method of constant stimuli [65]. In our case, the controlled stimulus was the actuator's driving pressure, which affected the experienced force, upon the finger motion from extension to flexion. Comparison tests were performed, presenting the user with consecutive pairs of stimuli, consisting of a reference stimulus and a comparison stimulus. Each subject was tested multiple times, experimenting with the following set of pressures (stimuli): 0, 0.5, 1, 1.5, 2, 2.5, and 3 bar. The midpoint intensity (1.5 bar) was used as a constant reference stimulus, as the constant stimuli test requires a consistent and symmetric distribution of all the comparison stimuli. Specifically, the test design necessitates equal spacing between the minimum and maximum applied pressures, as well as uniform increments between successive stimuli, to ensure reliable assessment of perceptual sensitivity. The test was performed according to the following procedural steps.

Firstly, the pressure was set to the reference value and the subject was requested to perform three cycles of finger motion from extension to flexion. Secondly, the pressure was changed to a comparison value (randomly chosen amongst the other six values of the set) and the subject was requested to perform other three cycles of finger motion. Then, the subject was asked whether during the second trial (three cycles with the comparison stimulus) the perceived force was higher or lower than that in the first trial (three cycles with the reference stimulus). Therefore, the test was of the kind known as two-alternative forced choice. This procedure was repeated an additional five times, by changing the comparison stimulus, randomly choosing it amongst the remaining values of the set. The random choice allowed for avoiding biasing/anticipation and habituation/adaptation effects.

It is worth noting that the subjects were requested to assess each perceived force only after three cycles of motion, as

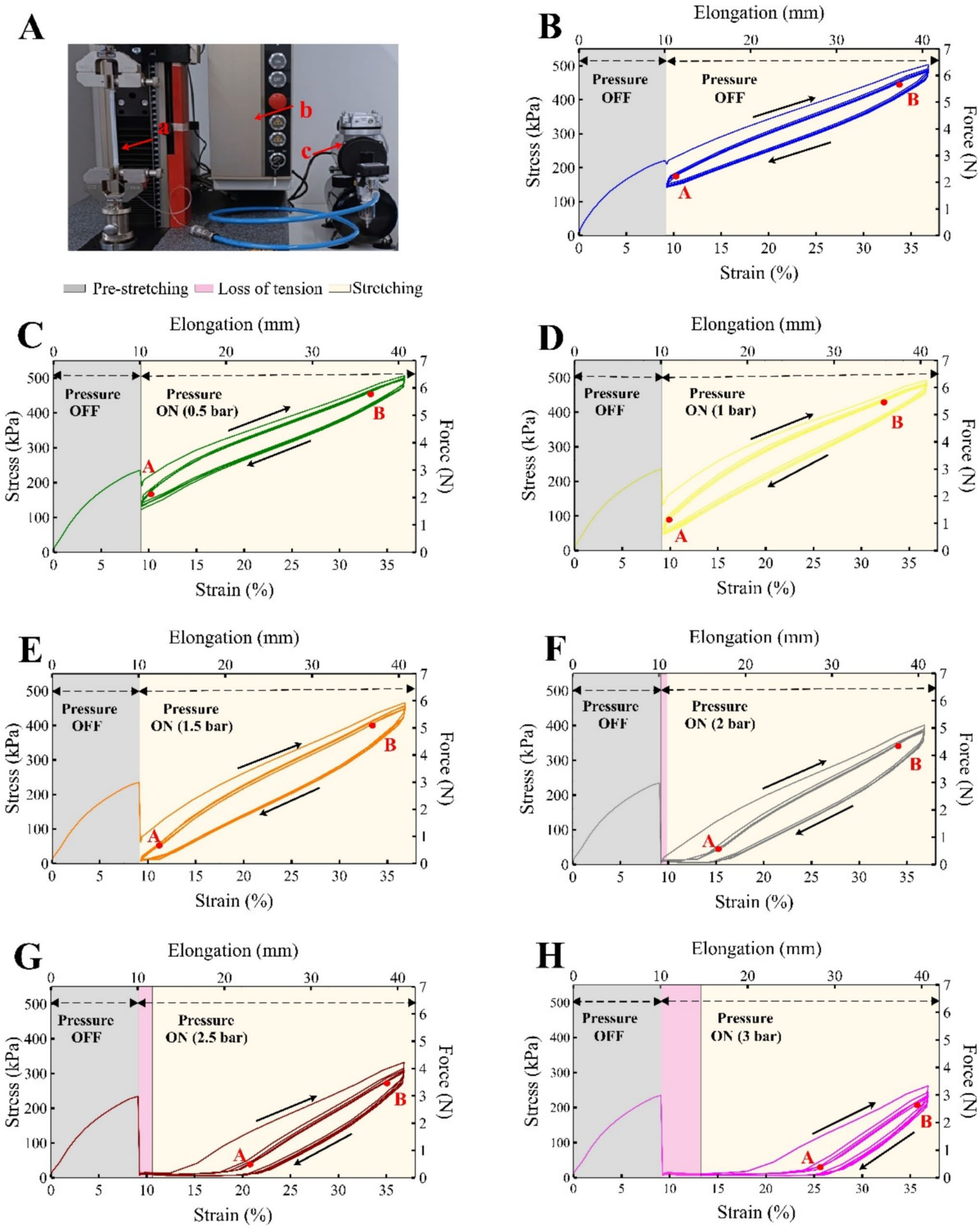
A
a
b
c
Pre-stretching
Loss of tension
Stretching
B
Elongation (mm)
Pressure OFF
Pressure OFF
Stress (kPa)
Force (N)
Strain (%)
C
Pressure OFF
Pressure ON (0.5 bar)
D
Pressure OFF
Pressure ON (1 bar)
E
Pressure OFF
Pressure ON (1.5 bar)
F
Pressure OFF
Pressure ON (2 bar)
G
Pressure OFF
Pressure ON (2.5 bar)
H
Pressure OFF
Pressure ON (3 bar)

◂**Fig. 4** Tensile mechanical testing of the pneumatic soft actuator: **A** Test setup showing the different parts of the system: **a** actuator, **b** dynamometer, **c** compressor. **B**–**H** Stress–strain and force–elongation co-plots, at different pressures. Each panel shows an initial pre-stretching phase (grey), followed by both a loss of tension phase (pink, not always visible) and a stretching phase (beige), during which five cycles of elongation and release were performed. Points A and B correspond to the minimum and maximum forces generated by the actuator during the 5th cycle of stretching, used to calculate its stiffness

preliminary evidence had shown that, in some cases, subjects needed more than one execution of movement to confidently appreciate differences in force.

This test was performed on 22 subjects, who did not report any diagnosed neuromuscular pathology. One of them was later excluded, because they did not complete the test. Out of the remaining 21 subjects, 13 were females aged between 21 and 45, and 8 were males aged between 24 and 65. The test was conducted in compliance with the guidelines of the Declaration of Helsinki and was approved by the Ethics Commission of the University of Florence (n. 442, 15 September 2025). Informed consent was obtained from all subjects.

Psychophysical Test on Null Force Perception

A second type of psychophysical test was conducted to assess the perceptual sensitivity to low forces, as follows. The experiment was performed with the finger in a maximally and constantly flexed position. According to a staircase method, the actuator's pressure was first gradually increased from 0 to 3.5 bar, to continuously reduce the perceived force from an initial maximum value, until the subject indicated (by saying "stop") that they no longer perceived any force on their finger. At this point, the pressure was gradually reduced, until the subject indicated that they once again sensed a force.

This procedure was repeated three additional times, with pressure being increased and decreased continuously, based on the subject's responses.

The test was performed on 14 subjects (a subset of those who had performed the first test). Out of them, 4 subjects were later excluded, for different reasons (two of them did not understand how to perform the task, and the other two produced unreliable data—outliers). Out of the remaining 10 subjects, 3 were females aged between 26 and 32 years, and 7 were males aged between 21 and 54 years.

Results

Stress–Strain Characterisation

The results of the tensile tests that mimicked the deformation experienced by the actuator within the splint whilst the finger was moved from extension to flexion, and vice-versa, are presented in Fig. 4.

In particular, the plots show the force–elongation curves corresponding to cyclic stretching and releasing, at different applied pressures within the range 0–3 bar. Indeed, following an initial pre-strain, the actuator was cyclically stretched and released five times to stabilise its hysteretic loop. The latter was caused by the constitutive elastomer's viscoelastic properties, as well as by possible additional mechanical losses introduced by structural effects, such as the Nylon coil sliding with friction on the tubes' surface. As revealed by the graphs, substantial stabilisation initiated after the 2nd cycle and was completed after the 4th cycle.

The plots also reveal that a pressure of 1.5 bar was able to cancel out the effect of pre-stretching in terms of force output, as at that pressure the force at pre-stretch (10 mm elongation) reverted to a null value (Fig. 4E). At lower pressures, the actuator retained at pre-stretch a non-null tensile force (panels B–D), whilst at higher pressures the actuator exhibited loss of tension, before generating again a non-null tensile force upon stretching (panels F–H). A loss of tension occurred because the actuator experienced bending, due to the significant pressurisation and according to its form factor.

For each pressure value P, within the 30 mm range of the actuator's elongation, we estimated the actuator's stiffness, as follows. Firstly, on the ascending part (stretching phase) of the stabilised (5th cycle) force-elongation loop, we identified the two points A and B (indicated in each panel of Fig. 4), corresponding to 10 and 90%, respectively, of the maximum force; secondly, we defined the stiffness as the slope of the line connecting A and B:

$$Stiffness(P) = \frac{F_B(P) - F_A(P)}{L_B - L_A}, \tag{2}$$

where L_A and L_B were the actuator's lengths in A and B, respectively, whilst F_A and F_B were the forces in A and B, respectively. Such a straightforward linearisation of the force–elongation curves (Fig. 4) to quantify the stiffness was motivated by the following consideration. We expect that the subjective evaluation of the resistance exerted by the splint upon the actuator's stretching was mostly determined by a perceptual assessment of the initial and final forces F_A and F_B, rather than a perceptually more complex evaluation of the continuously varying local slope of the force-elongation curve (i.e. the actual physical stiffness).

However, whilst up to the intermediate pressure (1.5 bar) the minimum force was rather evident (Fig. 4), at increasing pressures the loss of tension progressively made the minimum force more 'evanescent' (Fig. 4), i.e. more difficult to perceive. Therefore, to quantify the stiffness, we first defined (for any pressure value) a practical onset of the stretching phase, setting a threshold of 10% of the maximum force. Consistently, having excluded the initial 10% of the excursion range, we also excluded the final 10% of that range, such that the stiffness was estimated between 10 and 90%. This also allowed us to discard the steep increase of slope observed in each curve close to the maximum force (Fig. 4), which was significantly higher than the average slope throughout the 10–90% range, and therefore would have altered the assessment of the practically relevant stiffness throughout the largest part of the stretching phase.

The estimated stiffness is plotted in Fig. 5A, which shows a monotonic increase with the applied pressure.

Figure 5B represents a co-plot, as a function of the pressure, of the maximum stress and maximum force, which were achieved at the maximum elongation of 30 mm. As expected, an increasing pressurisation of the actuator caused a reduction in the force and stress required to elongate it by the same amount (30 mm), i.e. the actuator showed an equivalent softening.

Comparisons Between Experimental and Simulated Mechanical Responses

The finite element model exhibited good numerical stability throughout all simulation phases. No convergence issues were observed, despite the presence of large deformations and a nonlinear hyperelastic material response. Results of the finite element simulations are presented in Fig. 6, in comparison with the experimental measurements.

Overall, the simulations were found to be in rather good agreement with the measurements, as evident from the data at 0, 1, and 2 bar. However, a mismatch appeared at 3 bar (Fig. 6B, C). That discrepancy was likely due to the fact that, for the highest pressure, the actuator experimentally showed a loss of tension, as visible from the curve in Fig. 6B (the force remained null in the strain range 10 to 15%, approximately). Such a loss of tension, corresponding to an unstable behaviour, was not captured by the simulation, which therefore overestimated the reaction force.

Dynamic Psychophysical Test on Perceptual Differences in Force

The data gathered from the participants in the psychophysical test on perceptual differences in force were aggregated to create a psychometric curve, presented in Fig. 7.

The curve indicates the probability that the perceived comparison force was lower than the perceived reference force. The sigmoidal fitting of the data showed the classical expected trend in probability for a variable intensity of the stimulus, which in this experiment was the pressure. By setting a threshold probability to 50%, the corresponding threshold pressure, known as the point of subjective equality (PSE), was found to be ~ 1.5 bar (Fig. 7), i.e. almost exactly the reference value adopted in the test.

It should be noted that, as increasing pressures corresponded to decreasing forces, the low probability found at pressures lower than the reference one (Fig. 7) indicates that the subjects correctly perceived the comparison force as stronger than the reference one. This outcome reverted at pressures higher than the reference one, as in that range the

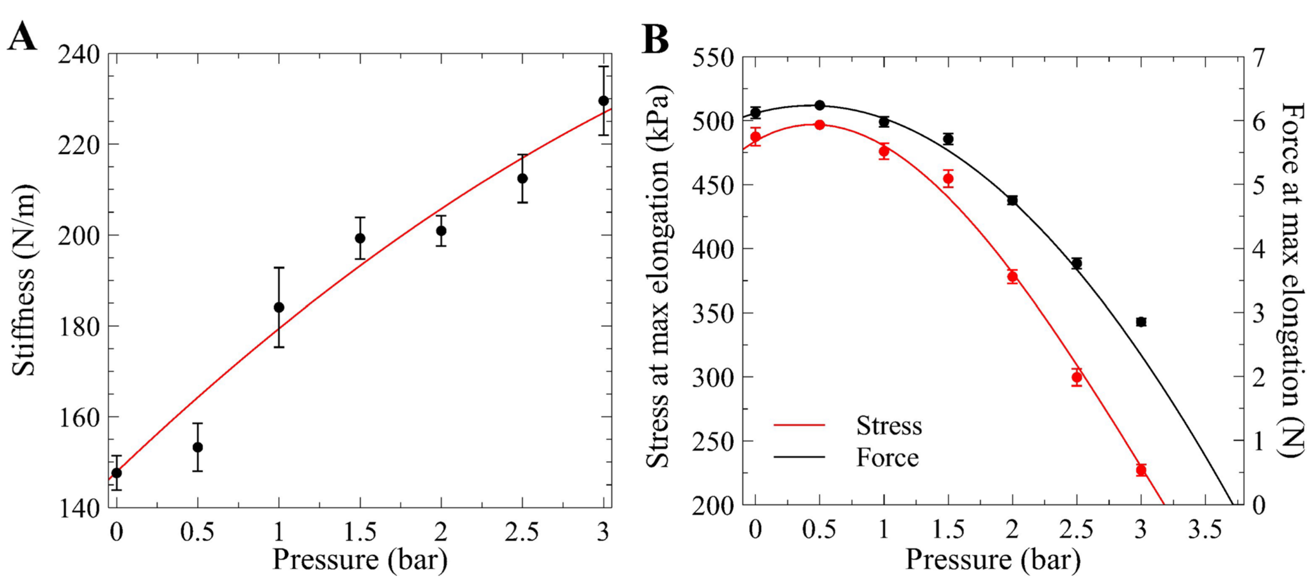

Fig. 5 **A** Actuator's stiffness as a function of its driving pressure; **B** Co-plots of the stress and force at the maximum elongation of 30 mm as functions of the pressure. The error bars represent the standard deviation amongst three actuator samples; fitting curves are used as a guide for the eye

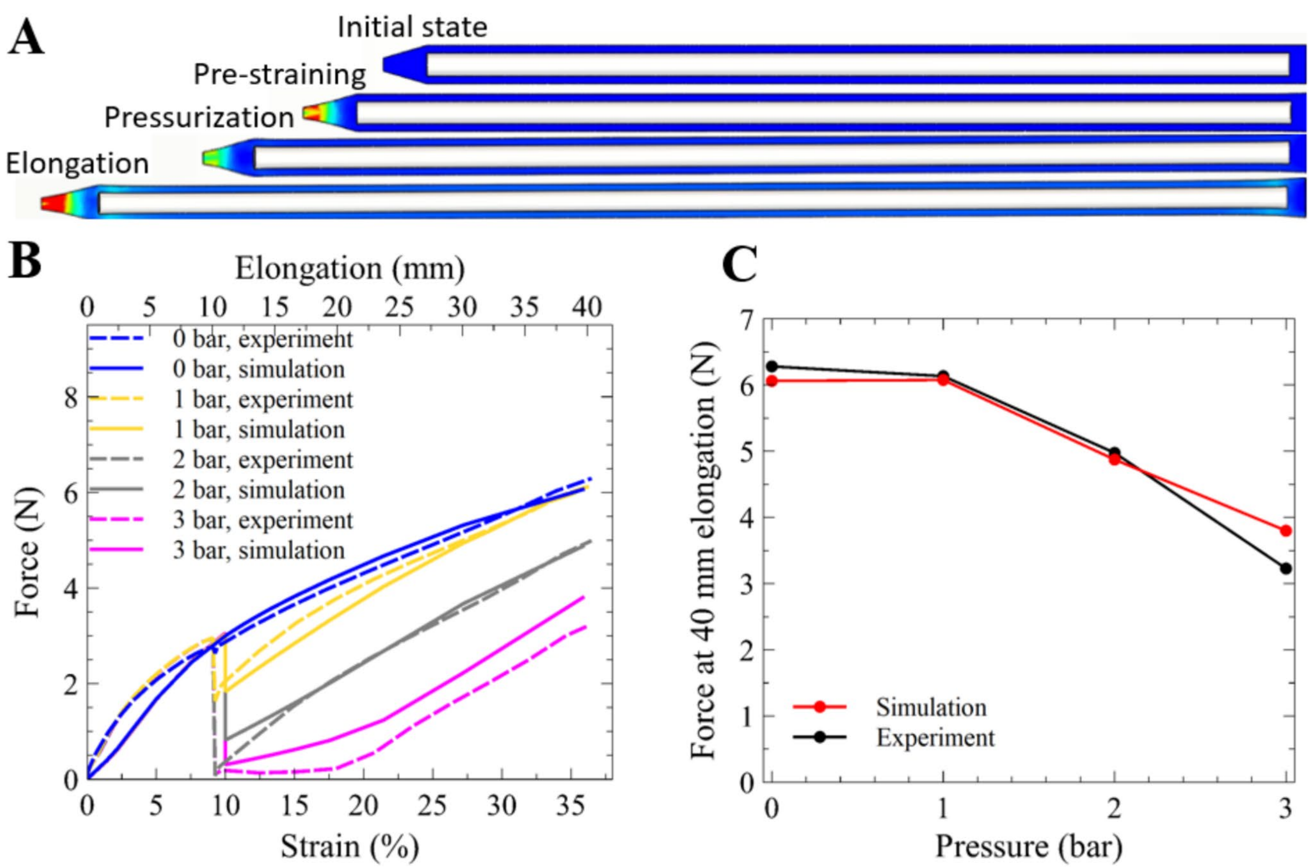

Fig. 6 **A** Finite element model of the actuator, shown at four stages of a quasi-static simulation: initial state (no pressure), 10 mm pre-strain, pressurisation, and 40 mm elongation. **B** Co-plots of simulated and experimental force–elongation curves, at different pressures. **C** Co-plots of simulated and experimental values of the maximum force generated by the actuator at an elongation of 40 mm, with different applied pressures

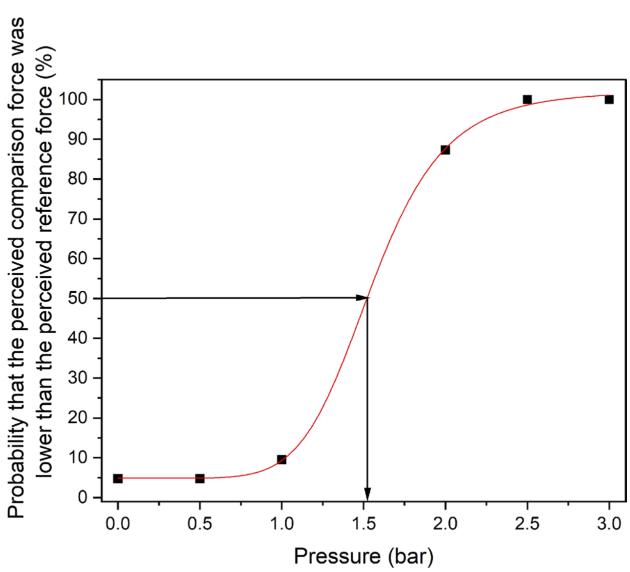

Fig. 7 Psychometric curve representing the results of the dynamic psychophysical test. A sigmoidal fitting curve is added as a guide to the eye, together with a threshold corresponding of 50% probability, to identify the corresponding threshold pressure from the fitting curve

comparison force was perceived as weaker than the reference one (Fig. 7).

The psychometric curve's slope was used to quantify the sensitivity to changes in the stimulus; in particular, the slope at 50% probability was found to be ~ 110 %/bar.

Static Psychophysical Test on Null Force Perception

The data gathered from the participants in the psychophysical test on null force perception are presented in Fig. 8.

In particular, for each subject, the histogram shows the force range recorded onboard the splint, when the pressure was increased up to the point when the subject reported a null force perception. The highest values at the initial null pressure are compared with the corresponding measurements (dots) taken from the actuator during its bench test. To ensure such comparisons of force, the actuator's elongation imposed onboard the splint by the finger flexion was measured and used to extrapolate from the bench test curves the corresponding force value.

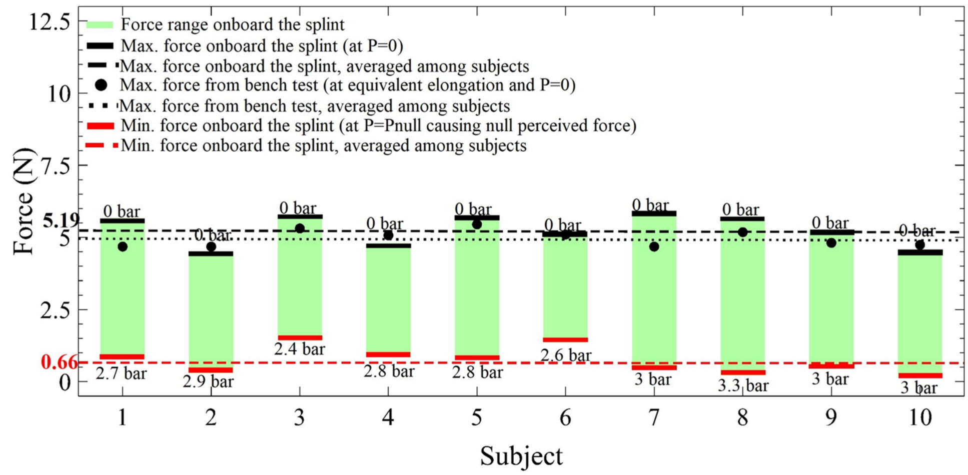

Fig. 8 Force values (averaged amongst four repeats, for each subject) measured onboard the splint during the static psychophysical test on null force perception and their comparison with force values measured during the mechanical bench tests (dots). Each green bar shows the force range onboard the splint when the pressure is increased from 0 bar to the value indicated at the lower end, which corresponds to a null perceived force

As indicated in the graph, the maximum force measured onboard the splint (at no pressure) averaged amongst the subjects was ~ 5.2 N, whilst the corresponding average maximum force in the bench tests was 5 N. This reveals that the finger flexion was consistent across the subjects and was properly captured by the load cell onboard the splint, in agreement with the stress-strain bench characterisation results.

The minimum averaged force measured onboard the splint when the subjects declared no perception of force was rather low (~0.7 N, with a standard deviation of 0.45), revealing a good accuracy of the system.

Discussion

The technology described in this article was inspired by earlier work from our group, which dealt with dynamic hand splints equipped with dielectric elastomer actuators (DEAs), consisting of either contractile folded units [61] or extending planar sheets [60]. Those investigations showed the possibility of using soft electrically tuneable actuators lodged onboard the splint, to control the force (and therefore also the stiffness) exerted by the device upon voluntary finger flexions. A similar approach was adopted more recently by Amin et al. [62], who used elongating spring-roll DEAs. Such DEAs had previously been used by Zhang et al. to develop another kind of system able to generate opposing forces against voluntary finger flexions, although in that case the actuators were arranged in the hand palm [63]. Whilst providing effective solutions to generate controllable counteractive forces suited to accomplish hand rehabilitation tasks, in all those previous works the most significant limitation was the need for high driving voltages.

To avoid that issue, the work described here introduced a dynamic splint based on soft pneumatic actuation, which made the system electrically safe, as well as capable of delivering significant forces, virtually limited only by the power of the external pneumatic driving unit. Moving the force generation site from the splint (as it was in the DEA-based prototypes) to an external unit represented the system's strength, as it removed performance-limiting constraints on the actuation technology. However, at the same time, that strategy also represented a weakness, as it increased the overall bulkiness and weight, and introduced acoustic noise (caused by the pneumatic driving unit). Therefore, as for any technological solution, the pneumatic device described in this work should be considered as a trade-off between pros and cons.

To accomplish a comparative analysis of our work with previously reported soft pneumatic actuation systems for the hand, the closest comparable solution is represented, to the best of our knowledge, by the study described by Phan et al. [50]. Whilst their system was conceived for grasping assistance (rather than dynamic splinting), and was hydraulically (rather than pneumatically) actuated, the actuator's configuration and working principle were analogous, consisting of depressurisations of soft tubing surrounded by a coil and connected to the finger via tendons. However, their tube was made of latex and the coil was metallic (steel), requiring a pressure of ~ 18.6 bar to achieve a 100% strain. The actuators employed in the system presented here were made of silicone, had a Nylon coil, and produced a ~ 22% strain at 3 bar. Keeping the actuation pressure limited as much as possible has important implications for the pneumatic driving unit, to reduce its size and increase its safety. The use of lightweight constitutive materials and compressed air (rather than liquids) is beneficial to reduce the total weight of the system, increasing its wearability and comfort.

In summary, this paper presents a dynamic hand splint, whose resistive force to voluntary finger movements can be controlled by a pneumatic actuator, which elongates upon pressurisation.

A dynamic psychophysical test on perceptual differences in force proved that subjects were able to reliably perceive differences in force, consistently with the driving pressure. Specifically, the sensitivity against variations in force intensity, quantified as the slope of the psychometric curve, was found to be ~ 110 %/bar at 50% probability.

A static psychophysical investigation provided insights into the maximum counteracting force exerted by the splint. Upon the finger's full flexion, the actuator exerted a maximum resistive force of ~ 5.2 N (averaged amongst 10 subjects), which was nulled (and was actually perceived by subjects as nearly null) when the pressure was increased from 0 to 3 bar. That force range was fully consistent with data gathered from a benchtop stress–strain characterisation of the actuator. This indicates that the actuator's arrangement onboard the splint did not introduce any constraint capable of significantly affecting the actuation performance.

Future developments might focus on improving the splint design, to make it lighter, more compact, and more comfortable. Moreover, it would be important to take advantage of the possibility of providing the actuator with self-sensing properties [54], to implement real-time stiffness control strategies.

Additional important developments should also consider a possible biomechanical modelling of the whole system, including both the splint and the biomechanical kinematic chain, starting from the finger skin, down to the tendons, muscles, and bones. Modelling should take into account imperfect adhesion between the fingertip and the plastic cap, such that the pulling force is expected to tilt, to some extent, the cap around the distal phalanx. Whilst we believe that such tilting is possible, and that it might significantly vary according to the individual fingertip anatomy, we have not investigated it so far. Such a variable tilting would change the angle of application of the force vector relative to the phalanx's main axis. Furthermore, such a variation might depend on the finger flexion angle, i.e. the finger movement. Modelling such effects would clarify how the finger motions are likely to solicit pressure/stress or stretch receptors in the muscles, tendons, joints, or skin. The resulting understanding of the involved biomechanical pathways would allow for formulating biomechanical interpretations of the outcomes of our psychophysical tests.

Supplementary Information The online version contains supplementary material available at https://doi.org/10.1007/s10439-026-04233-3.

Funding Open access funding provided by Università degli Studi di Firenze within the CRUI-CARE Agreement. Financial support from the European Commission's Marie Skłodowska-Curie Actions Doctoral Networks Programme (HORIZON-MSCA-2021, Project 101072920-SOFTWEAR), the Italian Ministry of University and Research (PNRR PE8 project "AGE-IT– Ageing well in an ageing society" CUP B83C22004800006 and PNC project "Fit4MedRob - Fit for Medical Robotics" grant PNC0000007) and Fondazione Cassa di Risparmio di Firenze, Italy (projects "HAPTICS", "REHub", "R3COVER", and "Lab Didattici Ingegneria Biomedica"") is gratefully acknowledged.

Declarations

Conflict of interest The authors have no relevant financial or non-financial interests to disclose.

Ethical Approval The study was approved by the Ethics Committee of the University of Florence (n. 442, 15 September 2025) and conformed to the ethical standards in the Declaration of Helsinki. All participants provided written, informed consent.

References

1. Duncan CC, Edgley SR. Upper limb orthoses for the stroke- and brain-injured patient. In: *Atlas of Orthoses and Assistive Devices*. Philadelphia: Elsevier; 2019. p. 146–156.e2. https://doi.org/10.1016/B978-0-323-48323-0.00013-5
2. Huang Y-C. Therapeutic efficacy of dynamic hand splints in spastic hemiparetic hands: a randomized controlled single-blind trial. RPS 49, 2021. https://doi.org/10.6315/tjpmr.202106_49(1).0006
3. Bianca, C., J. Machuki, and W. Chen. A dynamic splint for the treatment of spasticity of the hand after stroke – recognition of its design, functionality and limitations: a narrative review article. *J Neurol Neurorehabil Res*. 3:17–19, 2018.
4. Kerr, L., V. D. Jewell, and L. Jensen. Stretching and splinting interventions for poststroke spasticity, hand function, and functional tasks: a systematic review. *Am J Occup Ther*. 74:7405205050, 2020. https://doi.org/10.5014/ajot.2020.029454.
5. Jackman, M., I. Novak, and N. Lannin. Effectiveness of hand splints in children with cerebral palsy: a systematic review with meta-analysis. *Dev Med Child Neurol*. 56:138–147, 2013. https://doi.org/10.1111/dmcn.12205.
6. Kelly BM, Berenz T, Williams T. Orthoses for the burned hand. In: *Atlas of Orthoses and Assistive Devices*. Philadelphia: Elsevier; 2019. p. 170–175.e1. https://doi.org/10.1016/B978-0-323-48323-0.00015-9
7. Yang, Y.-S., Z. F. Emzain, and S.-C. Huang. Biomechanical evaluation of dynamic splint based on pulley rotation design for management of hand spasticity. *IEEE Trans Neural Syst Rehabil Eng*. 29:683–689, 2021. https://doi.org/10.1109/TNSRE.2021.3068453.
8. Pan M, Yuan C, Liang X, Dong T, Liu T, Zhang J, et al. Soft actuators and robotic devices for rehabilitation and assistance. *Adv Intell Syst* 4(4), 2021. https://doi.org/10.1002/aisy.202100140
9. Noronha, B., and D. Accoto. Exoskeletal devices for hand assistance and rehabilitation: a comprehensive analysis of

state-of-the-art technologies. *IEEE Trans Med Robot Bionics*. 3:525–538, 2021. https://doi.org/10.1109/TMRB.2021.3064412.
10. Kabir, R., M. Sunny, H. Ahmed, and M. Rahman. Hand rehabilitation devices: a comprehensive systematic review. *Micromachines*. 13:1033, 2022. https://doi.org/10.3390/mi13071033.
11. Zhang, Z., A. Calderon, X. Huang, and A. Huang. Research status and prospect of finger rehabilitation machinery. *Med Devices Evid Res*. 17:1–22, 2024. https://doi.org/10.2147/MDER.S429206.
12. Gherman, B., I. Zima, C. Vaida, P. Tucan, A. Pisla, I. Birlescu, et al. Robotic systems for hand rehabilitation—past, present and future. *Technologies*. 13:37, 2025. https://doi.org/10.3390/technologies13010037.
13. Gerez, L., J. Chen, and M. Liarokapis. On the development of adaptive, tendon-driven, wearable exo-gloves for grasping capabilities enhancement. *IEEE Robot Autom Lett*. 4:422–429, 2019. https://doi.org/10.1109/LRA.2019.2890853.
14. Serpelloni M, Tiboni M, Lancini M, Pasinetti S, Vertuan A, Gobbo M. Preliminary study of a robotic rehabilitation system driven by EMG for hand mirroring. In: 2016 IEEE *International Symposium on Medical Measurements and Applications (MeMeA)*; 2016. p. 1–6. https://doi.org/10.1109/MeMeA.2016.7533730
15. Alicea R, Xiloyannis M, Chiaradia D, Barsotti M, Frisoli A, Masia L. A soft, synergy-based robotic glove for grasping assistance. *Wearable Technol* 2, 2021. https://doi.org/10.1017/wtc.2021.3
16. In, H., B. B. Kang, M. Sin, and K.-J. Cho. Exo-Glove: a wearable robot for the hand with a soft tendon routing system. *IEEE Robot Autom Mag*. 22:97–105, 2015. https://doi.org/10.1109/MRA.2014.2362863.
17. Park, S., C. Meeker, L. M. Weber, L. Bishop, J. Stein, and M. Ciocarlie. Multimodal sensing and interaction for a robotic hand orthosis. *IEEE Robot Autom Lett*. 4:315–322, 2019. https://doi.org/10.1109/LRA.2018.2890199.
18. Kim, S., J. Lee, and J. Bae. Analysis of finger muscular forces using a wearable hand exoskeleton system. *J Bionic Eng*. 14:680–691, 2017. https://doi.org/10.1016/S1672-6529(16)60434-1.
19. Gobbo, M., P. Gaffurini, L. Vacchi, S. Lazzarini, J. Villafane, C. Orizio, et al. Hand passive mobilization performed with robotic assistance: acute effects on upper limb perfusion and spasticity in stroke survivors. *Biomed Res Int*. 2017:1–6, 2017. https://doi.org/10.1155/2017/2796815.
20. Milia, P., M. C. Peccini, F. De Salvo, A. Sfaldaroli, C. Grelli, G. Lucchesi, et al. Rehabilitation with robotic glove (Gloreha) in poststroke patients. *Digit Med*. 5:62–67, 2019. https://doi.org/10.4103/digm.digm_3_19.
21. Wang, Y., S. Zheng, J. Pang, S. Li, and J. Li. Design and experiment of a hand movement device driven by shape memory alloy wires. *J Robot*. 2021:1–13, 2021. https://doi.org/10.1155/2021/6611581.
22. Lee S-M, Shin G, Im H, Oh M, Castro Avalos S, Yoon M-J, et al. Feasibility of a warp-knitted shape memory alloy rehabilitation glove. *J Ind Text* 54, 2024. https://doi.org/10.1177/15280837241238446
23. Lai, Y.-J., L.-J. Yeh, and M.-C. Chiu. An experimental investigation on shape memory alloy dynamic splint for a finger joint application. *Sens Actuators A Phys*. 173:210–218, 2012. https://doi.org/10.1016/j.sna.2011.11.012.
24. Yao, Z., C. Linnenberg, A. Argubi-Wollesen, R. Weidner, and J. P. Wulfsberg. Biomimetic design of an ultra-compact and lightweight soft muscle glove. *Prod Eng*. 11:731–743, 2017. https://doi.org/10.1007/s11740-017-0767-y.
25. Saharan, L., M. J. de Andrade, W. Saleem, R. H. Baughman, and Y. Tadesse. iGrab: hand orthosis powered by twisted and coiled polymer muscles. *Smart Mater Struct*. 26:105048, 2017. https://doi.org/10.1088/1361-665X/aa8929.
26. Polygerinos P, Correll N, Morin SA, Mosadegh B, Onal CD, Petersen K, et al. Soft robotics: review of fluid-driven intrinsically soft devices; manufacturing, sensing, control, and applications in human-robot interaction. *Adv Eng Mater* 19, 2017. https://doi.org/10.1002/adem.201700016
27. Zhu, Y., W. Gong, K. Chu, X. Wang, Z. Hu, and H. Su. A novel wearable soft glove for hand rehabilitation and assistive grasping. *Sensors*. 22:6294, 2022. https://doi.org/10.3390/s22166294.
28. Zhang, X., and A. E. Oseyemi. A herringbone soft pneu-net actuator for enhanced conformal gripping. *Robotica*. 40:1345–1360, 2021. https://doi.org/10.1017/S0263574721001144.
29. Han, Y., Q. Xu, and F. Wu. Design of wearable hand rehabilitation glove with bionic fiber-reinforced actuator. *IEEE J Transl Eng Health Med*. 10:1–10, 2022. https://doi.org/10.1109/JTEHM.2022.3196491.
30. Zhang, Y., M. Orban, Y. Wu, C. Liu, J. Wang, M. Elsamanty, H. Yang, and K. Guo. A review of soft robotics and soft rehabilitation gloves: exploring alternative soft robots actuation techniques. *International Journal of Intelligent Robotics and Applications*. 9(4):1368–1393, 2025. https://doi.org/10.1007/s41315-025-00474-y.
31. Jiang Y, Chen D, Liu P, Jiao X, Ping Z, Xu Z, et al. Fishbone-inspired soft robotic glove for hand rehabilitation with multi-degrees-of-freedom. In: *2018 IEEE International Conference on Soft Robotics (RoboSoft)*; 2018. p. 394–399. https://doi.org/10.1109/RoboSoft.2018.8404951
32. Wang, J., Y. Fei, and W. Pang. Design, modeling, and testing of a soft pneumatic glove with segmented pneunets bending actuators. *IEEE/ASME Trans Mechatron*. 24:990–1001, 2019. https://doi.org/10.1109/TMECH.2019.2911992.
33. Ramos, O., Múnera, M., Moazen, M., Wurdemann, H., & Cifuentes, C. A. (2022). Assessment of Soft Actuators for Hand Exoskeletons: Pleated Textile Actuators and Fiber-Reinforced Silicone Actuators. *Frontiers in Bioengineering and Biotechnology*, 10. https://doi.org/10.3389/fbioe.2022.924888
34. Lv, Y., Geng, Z., Wu, H., He, Y., & Lv, Z. (2025). Design and experimentation of the nested pneumatic soft actuator for hand exoskeleton. *Journal of Engineering and Applied Science*, 72(1). https://doi.org/10.1186/s44147-025-00704-x
35. Hong TH, Park SH, Park JH, Paik NJ, Park YL. Design of pneumatic origami muscle actuators (POMAs) for a soft robotic hand orthosis for grasping assistance. In: *2020 3rd IEEE International Conference on Soft Robotics (RoboSoft)*; 2020 May; New Haven, CT, USA. IEEE; 2020. p. 627–632. https://doi.org/10.1109/RoboSoft48309.2020.9115983
36. Yap, H. K., P. M. Khin, T. H. Koh, Y. Sun, X. Liang, J. H. Lim, et al. A fully fabric-based bidirectional soft robotic glove for assistance and rehabilitation of hand impaired patients. *IEEE Robot Autom Lett*. 2:1383–1390, 2017. https://doi.org/10.1109/LRA.2017.2669366.
37. Cappello, L., J. T. Meyer, K. C. Galloway, J. D. Peisner, R. Granberry, D. A. Wagner, et al. Assisting hand function after spinal cord injury with a fabric-based soft robotic glove. *J Neuroeng Rehabil*. 15:1–10, 2018. https://doi.org/10.1186/s12984-018-0391-x.
38. Polygerinos, P., Z. Wang, K. C. Galloway, R. J. Wood, and C. J. Walsh. Soft robotic glove for combined assistance and at-home rehabilitation. *Robot Auton Syst*. 73:135–143, 2015. https://doi.org/10.1016/j.robot.2014.08.014.
39. Wang F, Wang H, Luo J, Kang X, Zhang X, Chen L, et al. Design and research of a soft hand rehabilitation robot with multiple training modes. In: *2022 3rd International Conference on Computing, Networks and Internet of Things (CNIOT)*; 2022. p. 171–175. https://doi.org/10.1109/CNIOT55862.2022.00037
40. Guo, N., Z. Sun, X. Wang, E. H. K. Yeung, M. K. T. To, X. Li, et al. Simulation analysis for optimal design of pneumatic

bellow actuators for soft-robotic glove. *Biocybern Biomed Eng*. 40:1359–1368, 2020. https://doi.org/10.1016/j.bbe.2020.08.002.

41. J, A., & Thomas, J. (2025). Soft Pneumatic Exoskeleton Glove with Feedback Control for Precise Rehabilitation Training. In 2025 Advanced Computing and Communication Technologies for High Performance Applications (ACCTHPA) (pp. 1–6). IEEE. *2025 Advanced Computing and Communication Technologies for High Performance Applications* (ACCTHPA). https://doi.org/10.1109/accthpa65749.2025.11168715
42. Tejada, J. C., Toro-Ossaba, A., Valencia, S., Gallego, N., Jaramillo-Tigreros, J. J., Hernandez-Martinez, E. G., & López-González, A. (2024). Soft Robotic Hand Exoskeleton with Enhanced PneuNet-Type Pneumatic Actuators for Rehabilitation and Movement Assistance. *Journal of Robotics*, 2024(1). https://doi.org/10.1155/2024/5815358
43. Ridremont, T., I. Singh, B. Bruzek, A. Jamieson, Y. Gu, R. Merzouki, and M. B. J. Wijesundara. Pneumatically Actuated Soft Robotic Hand and Wrist Exoskeleton for Motion Assistance in Rehabilitation. *Actuators*. 13(5):180, 2024. https://doi.org/10.3390/act13050180.
44. Kladovasilakis, N., I. Kostavelis, P. Sideridis, E. Koltzi, K. Piliounis, D. Tzetzis, and D. Tzovaras. A Novel Soft Robotic Exoskeleton System for Hand Rehabilitation and Assistance Purposes. *Applied Sciences*. 13(1):553, 2022. https://doi.org/10.3390/app13010553.
45. Kalita, B., A. Leonessa, and S. K. Dwivedy. A review on the development of pneumatic artificial muscle actuators: force model and application. *Actuators*. 11:288, 2022. https://doi.org/10.3390/act11100288.
46. Hassanin, A.-F., D. Steve, and N.-M. Samia. A novel, soft, bending actuator for use in power assist and rehabilitation exoskeletons. *IEEE/RSJ International Conference on Intelligent Robots and Systems (IROS)*. 2017:533–538, 2017. https://doi.org/10.1109/iros.2017.8202204.
47. Shiota K, Tarvainen TVJ, Sekine M, Kita K, Yu W. Development of a robotic thumb rehabilitation system using a soft pneumatic actuator and a pneumatic artificial muscles-based parallel link mechanism. *Advances in Intelligent Systems and Computing* 2017;525–37. https://doi.org/10.1007/978-3-319-48036-7_38.
48. Koizumi, S., T.-H. Chang, H. Nabae, G. Endo, K. Suzumori, M. Mita, et al. Soft Robotic Gloves with Thin McKibben Muscles for Hand Assist and Rehabilitation. *IEEE/SICE International Symposium on System Integration (SII)*. 2020:93–98, 2020. https://doi.org/10.1109/sii46433.2020.9025832.
49. Skaramagkas, V., G. Andrikopoulos, and S. Manesis. Towards essential hand tremor suppression via pneumatic artificial muscles. *Actuators*. 10:206, 2021. https://doi.org/10.3390/act10090206.
50. Koizumi, S., Chang, T.-H., Nabae, H., Endo, G., Suzumori, K., Mita, M., Saitoh, K., Hatakeyama, K., Chida, S., & Shimada, Y. (2020). Soft Robotic Gloves with Thin McKibben Muscles for Hand Assist and Rehabilitation. In 2020 IEEE/SICE International Symposium on System Integration (SII) (pp. 93–98). 2020 IEEE/SICE *International Symposium on System Integration (SII)*. IEEE. https://doi.org/10.1109/sii46433.2020.9025832
51. Takahashi, N., Takahashi, H., & Koike, H. (2019). Soft Exoskeleton Glove Enabling Force Feedback for Human-Like Finger Posture Control with 20 Degrees of Freedom. In 2019 IEEE World Haptics Conference (WHC) (pp. 217–222). 2019 IEEE *World Haptics Conference (WHC)*. IEEE. https://doi.org/10.1109/whc.2019.8816142
52. Potnik, V., G. Frediani, and F. Carpi. How to easily make self-sensing pneumatic inverse artificial muscles. *Biomimetics*. 9:177, 2024. https://doi.org/10.3390/biomimetics9030177.
53. Hawkes, E. W., D. L. Christensen, and A. M. Okamura. Design and implementation of a 300% strain soft artificial muscle. *IEEE International Conference on Robotics and Automation (ICRA)*. 2016:4022–4029, 2016. https://doi.org/10.1109/icra.2016.7487592.
54. Lorenzon L, Beccali G, Maselli M, Cianchetti M. A Self-sensing inverse pneumatic artificial muscle. 2022 IEEE *5th International Conference on Soft Robotics* (RoboSoft) 2022:817–22. https://doi.org/10.1109/robosoft54090.2022.9762204.
55. Phan, P. T., M. T. Thai, T. T. Hoang, N. H. Lovell, and Do. T. Nho. HFAM: Soft hydraulic filament artificial muscles for flexible robotic applications. *IEEE Access*. 8:226637–226652, 2020. https://doi.org/10.1109/access.2020.3046163.
56. Sandoval-Castro, X. Y., Cortes-Gonzalez, J. G., Ruiz-Torres, M. F., Castillo-Castaneda, E., & Laribi, M. A. (2025). Enhancing dexterity: Soft pneumatic actuation utilizing granular jamming for a human finger flexo-extension. *Wearable Technologies*, 6. https://doi.org/10.1017/wtc.2024.29
57. Opheim, A., A. Danielsson, M. Alt Murphy, H. C. Persson, and K. S. Sunnerhagen. Upper-Limb Spasticity During the First Year After Stroke. *American Journal of Physical Medicine & Rehabilitation*. 93(10):884–896, 2014. https://doi.org/10.1097/phm.0000000000000157.
58. Carpi, F., G. Frediani, C. Gerboni, J. Gemignani, and D. De Rossi. Enabling variable-stiffness hand rehabilitation orthoses with dielectric elastomer transducers. *Medical Engineering & Physics*. 36:205–211, 2014. https://doi.org/10.1016/j.medengphy.2013.10.015.
59. Carpi F, Mannini A, & De Rossi D. (2008, April). Elastomeric contractile actuators for hand rehabilitation splints. *In Electroactive polymer actuators and devices (EAPAD)* 2008 (Vol. 6927, pp. 37–46). SPIE
60. Amin, H., S. F. M. Assal, and H. Iwata. A new hand rehabilitation system based on the cable-driven mechanism and dielectric elastomer actuator. *Mechanical Sciences*. 11(2):357–369, 2020. https://doi.org/10.5194/ms-11-357-2020.
61. Zhang R, Lochmatter P, Kunz A, & Kovacs G. (2006). Spring roll dielectric elastomer actuators for a portable force feedback glove. In Y. Bar-Cohen (Ed.), SPIE *Proceedings. Smart Structures and Materials*. SPIE. https://doi.org/10.1117/12.658524
62. Fess, E. E., K. S. Gettle, J. Strickland, and L. M. Barber. Hand splinting—principles and methods. *Plastic and Reconstructive Surgery*. 69(2):373, 1982.
63. Brand, P. W. The forces of dynamic splinting: ten questions before applying a dynamic splint to the hand. In: Rehabilitation of the Hand: Surgery and Therapy, 4th ed., edited by J. M. Hunter, E. J. Mackin, and A. D. Callahan. St. Louis: Mosby, 1995, pp. 1581–1587.
64. Silva S, NPD N, Mattar Jr R, Bolliger Neto R, Pereira CAM. Measurement of the flexing force of the fingers by a dynamic splint with a dynamometer. *Clinics*. 2005;60:381–8. https://doi.org/10.1590/s1807-59322005000500006.
65. Jones, L. A., and H. Z. Tan. Application of psychophysical techniques to haptic research. *IEEE Trans Haptics*. 6:268–284, 2013. https://doi.org/10.1109/toh.2012.74.